buildings

MDPI

Article

Evaluation of Damage Limit State for RC Frame Based on FE Modeling

Stefanus Adi Kristiawan [1,*], Isyana Ratna Hapsari [2], Edy Purwanto [2] and Marwahyudi Marwahyudi [3]

[1] SMARTCrete Research Group, Civil Engineering Department, Sebelas Maret University, Surakarta 57126, Indonesia
[2] Civil Engineering Department, Sebelas Maret University, Surakarta 57126, Indonesia; isyanahapsari@student.uns.ac.id (I.R.H.); edypurwanto@student.uns.ac.id (E.P.)
[3] GFY Research Group, Universitas Sahid Surakarta, Surakarta 57144, Indonesia; yudhie_dsg@student.uns.ac.id
* Correspondence: s.a.kristiawan@ft.uns.ac.id

Abstract: Many damage limit states have been defined to characterize the extent of damages occurred in RC frame. Some of the damage limit states are defined by models that relate the limit states with the control points. Both control points and the limit state are expressed in term of response quantities. This research aims to evaluate the validity of such models by identifying the defined damage limit state with the corresponding damage based on FE modeling. The FE modeling provides a direct link between the damage and the response quantities. This link can be exploited as a basis for the evaluation. Based on the evaluation, this study proposed modified damage limit states. The response quantities with its corresponding progressive damage from FE simulation will also be used to inspect whether damage that can be expected to occur in the model structure is within the range estimated by the code based approach (CBA) damage limit state. Finally, fragility curves are constructed to assess the probability of the expected damage in the model structure under Design Basis Earthquake (DBE) and Maximum Considered Earthquake (MCE) scenarios. Utilizing the proposed damage limit states, the most probable damage in the structure falls in the category of slight if an earthquake at a level of DBE or MCE strikes the structure. However, at MCE level the probability of moderate damage attains 35%, or an increase by 23% compared to the DBE level.

Keywords: damage; FE modeling; fragility; limit state; RC frame; response

check for updates

Citation: Kristiawan, S.A.; Hapsari, I.R.; Purwanto, E.; Marwahyudi, M. Evaluation of Damage Limit State for RC Frame Based on FE Modeling. *Buildings* **2022**, *12*, 21. https://doi.org/10.3390/buildings12010021

Academic Editor: Humberto Varum

Received: 1 December 2021
Accepted: 27 December 2021
Published: 29 December 2021

Publisher's Note: MDPI stays neutral with regard to jurisdictional claims in published maps and institutional affiliations.

Copyright: © 2021 by the authors. Licensee MDPI, Basel, Switzerland. This article is an open access article distributed under the terms and conditions of the Creative Commons Attribution (CC BY) license (https://creativecommons.org/licenses/by/4.0/).

1. Introduction

The safety of buildings in earthquake-prone areas is a serious concern for stakeholders. Assessing the seismic performance of these buildings can provide an indication of the extent of damages that may occur in the future event of earthquake. Assessment may be carried out on large scale, covering buildings in a specific area or on single scale of building. For the first case, some literatures use simplified indexes that imply the safety of the buildings to be used for rapid evaluation [1–4]. A rapid evaluation method is developed to minimize the need of resources for the evaluation of the buildings in great numbers. However, the simplicity of the method may not yield a quite reliable result in certain case as noted by Ozmen [5]. Currently, machine learning is also being employed to rapidly estimate building vulnerability at large scale based on certain attributes data [6,7]. Meanwhile, for the case of assessing a single building, it is possible to perform more detailed analysis in order to observe the full seismic response of the investigated building. The response can be exploited further to determine the earthquake damage scenario of the building in terms of fragility, vulnerability or others [8–12].

Seismic fragility can be defined as the proneness of a structural component or a system to fail to perform satisfactorily under a predefined limit state when subjected to an extensive range of seismic action [13]. The precise definition of limit state will influence the accuracy of the seismic fragility assessment of the building. The definition of limit

state for the purpose of fragility assessment can be associated with the damage phenomena and/or damage parameters which account for the ductile or brittle mechanism [14–16]. Examples of various damage phenomena that may be observed in RC frame include concrete cracking and, in later stages, concrete crushing. Concrete crushing begins with spalling of concrete cover. After spalling, other failure modes may precede the crushing of concrete core, for example buckling and possible fracture of longitudinal reinforcement, or loss of anchorage. Damage can also be expressed in term of damage parameters such as strain (compressive/tensile), rotation, horizontal displacement, inter-story drift, floor acceleration, etc. [14–16].

Figure 1 provides an illustration of different stages of damage which affect the global behavior (in term of load carrying capacity-displacement relationship) of ductile RC frame. The damage is characterized by gradual phenomena from concrete cracking to buckling of rebars along with failing of covering concrete. Each damage stage is set as a damage class threshold. Originally, the curve was used to assess the residual seismic capacity ratio index R when damage class (defined according to Ohkubo [17]) in a building after earthquake have been identified. The index R is calculated as the ratio of seismic capacity index of post-damaged to that of pre-damaged condition. The concept and detail procedure for calculating seismic capacity index can be found in the cited literatures [18,19]. The use of the curve can be expanded to define damage state/class threshold that are expressed with other engineering demand parameters (EDPs) such as ductility factor, drift ratio, etc.

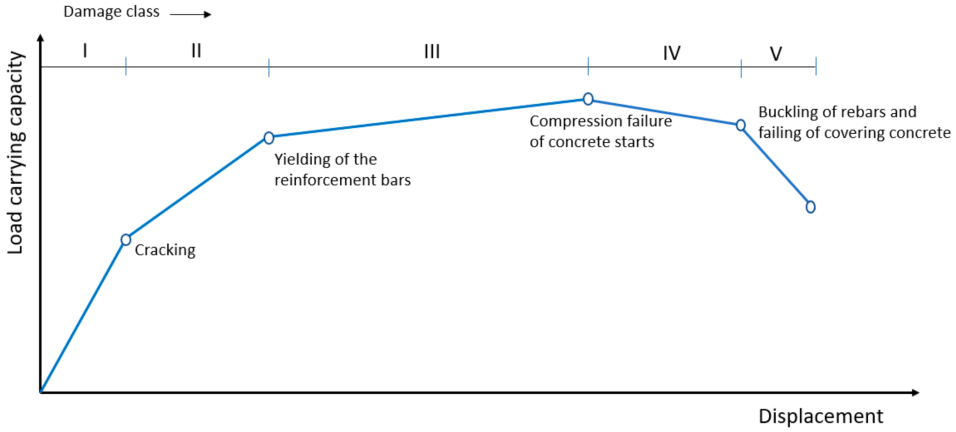


Figure 1. Idealized lateral forced-displacement relationships and damage class for ductile member [18].

The most important point that needs to be emphasized with regard to Figure 1 is the relationship between damage characteristics, EDP, and damage state. The relationship forms a basis for defining the damage limit state. The damage characteristics describe the physical damage that may be quantified in term of crack width of concrete, yield strain of reinforcing bar, and other observed physical damages. The shape of the load-displacement (or moment-curvature) curve is linked with the degree of physical damages. Hence, deformation quantities associated to the curve such as strain, displacement, rotation, etc., can be selected as damage parameters. Various EDPs are defined on the basis of these damage parameters. Based on the degree of physical damage and/or criteria of EDP, limit states are established to classify damage into various levels of damage state. The following sub section briefly review some approaches to define the damage limit state. At the end, the advantage of FE modeling is highlighted to propose the use of FE modeling for defining the damage limit state.

1.1. Damage Characterization and Damage Limit State

Researchers have carried out laboratory investigations to determine the seismic response of structures as well as observed the progressive damage that accompanied them. The results were taken into account for defining the damage limit state. Hamid and Mohamad [20] tested a full-scale double-story residential house under quasi-static lateral

cyclic loading. The building represented a reinforced concrete frame with unreinforced masonry infills walls type. Visual observations on the structural damages were recorded such as cracks width on the wall-column interface, crack propagations on the column, spalling and crushing of concrete. The observed damages were used to classify damage limit state of the structure based on the percentage of drift and the upper limit of the ductility factor. Carillo and Alcocer [21,22] investigated response of cantilever walls under quasistatic (monotonic and reversed-cyclic) and dynamic (shaking table) loading. They proposed tri-linear model for estimating the global load-displacement of this building type. The model was characterized by three limit states, i.e., diagonal shear cracking, peak shear strength, and ultimate deformation capacity. The acceptance limits were quantified by drift ratio, residual crack width, and residual damage index. Further work by Carillo, Dominguez, and Prado [23] proposed quantification of empirical damage index based on fractal dimension of cracking. In their work, damage was characterized by pattern and distribution of cracks. The proposed damage index is associated to limit states, so it can be employed for rapid estimation of damage level of the mentioned building type subjected to seismic demands. Ning et al. [24] investigated seismic performance of RC infills walls. The walls were made from Aerated Lightweight Concrete (ALC). The study observed the sequence of damage (crack width and intensity) and the corresponding drift ratio of the RC infill walls with various wall variables (with full-filled infill, with large opening, and with eccentric door openings). The results indicated the difference damage limit state for each type of infill wall. Ahmad et al. [25] presented lateral load-displacement response of code compliant and non-compliant RC special moment resisting frames under shaking table test. The observed gradual stages of damage were plotted in the response curves. The damage phenomena were labelled on the basis of the observed concrete cracking and spalling. There was no direct observation of strain in the reinforcing bars which otherwise would be useful to identify damage limit state corresponding to yielding of the reinforcing bars.

The biggest advantage of using experimental results is a direct correlation between the observed damages and the seismic response parameters. However, there are some technical constraints (e.g., lack of equipment to measure the detailed damage indices) as well as large financial costs that can affect how suitably the laboratory experiment is carried out. However, despite the limitations the observed physical damage phenomena from the test is required to assist in verifying the specified damage limit state, especially when the damage state in non-typical structure has to be determined [26,27].

1.2. Analytical Approach for Defining Damage Limit State

An analytical method (e.g., pushover analysis or dynamic analysis) can be employed to generate seismic response of RC frame structure. Most analytical methods are performed on the basis of member-type model where the finite element typically coincides with the actual structural member. Various response quantities both at member and global level can be expected from this type of analysis, including deformation, plastic hinge rotation, and curvature. Cracking and spalling of concrete are not part of the results of this model analysis. Thus, damage can only be identified and quantified based on the available response quantities as stated above.

The first things that needs to be identified from the seismic response are the yield and ultimate point, which are commonly referred to as the control points. The yield point equals the capacity of the building before structural system has developed nonlinear response, while the ultimate point is the capacity of the building when the global structural system has reached a plastic state. The control points may be identified graphically based on engineering judgments. More strict definition of the points has been suggested in some literatures. For example, Dimova and Negro [28] employed the concept of reduced stiffness equivalent elasto-plastic yield and equivalent elasto-plastic energy absorption. In these concepts, ultimate point is determined when the peak load drops at 15%. Other literature proposed a maximum cord rotation as a criterion [29].

Another points in the seismic response curve that represents the degree of damage between yielding and ultimate limit state need to be estimated from the control points. For this purpose, an appropriate damage model is needed to relate the response quantities with the estimated damage. Park and Ang [30] proposed a damage model to express the expected damage in RC as a function of maximum deformation and hysteretic energy. The maximum deformation consists of deformation due to flexural, elastic and inelastic shear, and slip (bond failure). The form of Park-Ang damage model has been used by some researchers to assess damage in RC. Kappos [14] evaluated the importance of the energy term of Park-Ang model where the deformation and energy term were represented by rotation and product of moment-rotation, respectively. He noted that the contribution of energy term is minor. Fu and Liu [31] took into account the influence of displacement amplitude and load sequence to modify the Park-Ang model. The damage indice of Park-Ang and its variations (modification) have been correlated with the seismic parameters to estimate the destructive effect of ground motion on RC building [15,32,33].

Damage indices obtained by Park-Ang model have been used to define damage limit state and adopted as one of the methods to develop fragility curve in RISK-EU WP4 [34]. The same document also suggests threshold value of damage states (*DS*0 to *DS*4) based on the displacement as shown in Equation (1).

$$\left.\begin{array}{c} DS0 = \Delta < 0.7\Delta_y \\ DS1 = 0.7\Delta_y < \Delta < 0.7\Delta_y + 0.05(\Delta_{uy}) \\ DS2 = 0.7\Delta_y + 0.05(\Delta_{uy}) < \Delta < 0.7\Delta_y + 0.20(\Delta_{uy}) \\ DS3 = 0.7\Delta_y + 0.20(\Delta_{uy}) < \Delta < 0.7\Delta_y + 0.50(\Delta_{uy}) \\ DS4 = 0.7\Delta_y + 0.50(\Delta_{uy}) < \Delta < 0.7\Delta_y + 1.00(\Delta_{uy}) \\ \Delta_{uy} = 0.9\Delta_u - 0.7\Delta_y \end{array}\right\} \quad (1)$$

where Δ_y and Δ_u are displacement at yielding reinforcement and ultimate, respectively. These two points are referred to as control points.

Vargas et al. [35] adopted Equation (2) of RISK-EU WP4 [34] to estimate four levels of damage limit state (*DS*1 to *DS*4) of RC frame.

$$\left.\begin{array}{l} DS1 = 0.7D_y \\ DS2 = D_y \\ DS3 = D_y + 0.25(D_u - D_y) \\ DS4 = D_u \end{array}\right\} \quad (2)$$

where D_y and D_u are spectral displacement corresponding to two control points in the capacity spectrum curve at yielding (A_y, D_y) and at ultimate (A_u, D_u) point, respectively. The control points can also be estimated using Equation (3) [34]:

$$\left.\begin{array}{l} A_y = S_{ay} = \frac{C_s\gamma}{\alpha_1} \\ D_y = S_{dy} = \frac{A_y}{4\pi^2}T^2 \\ A_u = S_{au} = \lambda\frac{C_s\gamma}{\alpha_1} \\ D_u = S_{du} = \lambda\mu\frac{C_s\gamma}{\alpha_1}\frac{T^2}{4\pi^2} \end{array}\right\} \quad (3)$$

where C_s, T, α, μ, λ, and γ are design strength, typical elastic period of the structure, fraction of building weight effective in the pushover mode, ductility factor, over strength factor relating yield strength to design strength, and over strength factor relating ultimate strength to yield strength, respectively. Equation (3) is similar to that of Hazus-MH 2.1 AEBM [36].

Hazus-MH 2.1 AEBM [36] provides another guideline to graphically determine the control points based on a set of rules and judgments. The document recognizes three possible capacity curves, i.e., capacity curve for a structure with saw-tooth, brittle, and ductile force-deflection behavior where different ultimate limit point is applied for each curve. Once the control points have been determined, the damage limit state (medians value) can be defined. Selection of damage-state medians should be consistent with the broad descriptions of structural damage given in the Hazus-MH 2.1 Technical Manual [37]. The detail procedure can be referred to the mentioned literature [36].

Naderpour and Mirrashid [38] selected the shear capacity, the moment capacity, and the shear strength, for beams, columns, and joints, respectively, for defining the damage state. The capacity is obtained from pushover analysis which then converted into demand ratio vs response ratio. The demand ratio represents the ratio of load/ultimate load or moment/ultimate moment, while the response ratio corresponds to the ratio of displacement/ultimate displacement. The corresponding points of damage states are determined using procedure given in the mentioned literature. The proposed damage states can be predicted based on the observed damages of beams, columns, and joints, simultaneously.

1.3. Code Based Approach (CBA) Damage Limit State

The capacity curve model in which the model parameters (Equation (3)) are estimated based on expert judgement of C_s, γ, λ, μ and T as prescribed by seismic codes and other accompanied standards is referred to as code-based approach (CBA) capacity. Examples of damage limit state derived from CBA capacity is Hazus-MH2.1.

Hazus-MH 2.1 Technical Manual [37] classified the damage state of structural system into 4 (four) levels where the extent of damage at each level is controlled by inter-story drift ratio as EDP. The drift threshold value of each damage state also takes into account the model building type (including height) and the seismic design level. The document covers 16 basic model building types, three categories of height, and four levels of design code. Combining the variations of building type, building height, and design code level render 128 building classes along with the specified damage states limit. For the case of RC frame that has been designed following high, medium, and low code level, the drift limit of the four damage states is presented in Table 1.

Table 1. The damage limit state of RC frame for low height building (Hazus-MH 2.1) [37].

Design Level	Interstory Drift at Threshold of Damage State (%)			
	Slight	**Moderate**	**Extensive**	**Complete**
High code	0.0050	0.0100	0.0300	0.0800
Medium code	0.0050	0.0087	0.0233	0.0600
Low code	0.0050	0.0080	0.0200	0.0500

FEMA P-58 [39] provides fragility database specifying the damage states that a given component can take, the demand parameter (e.g., story drift ratio) which predicts that damage, and provides a fragility function for predicting occurrence or exceedance of that damage state. The FEMA P-58 fragility database was generated from testing specimens covering a wide range of building types. It included six RC frame types corresponding to six design levels. Three of the RC frames are representative of RC frame which is designed conforming ACI 318 designs for low, medium, and high seismicity, respectively. Table 2 indicates the corresponding EDP that represents the damage limit state of these three RC frames along with its total dispersion value, β. For low code design, the damage state is only stratified into three classes i.e., *DS*1 to *DS*3, which means the building is expected to experience complete damage at *DS*3.

Table 2. The damage limit state for RC frame according to FEMA P-58 [39].

Design Level	Story Drift Ratio of the Median Demand, θ and the Corresponding Fragility Parameters, β							
	Slight (*DS*1)		**Moderate (*DS*2)**		**Extensive (*DS*3)**		**Complete (*DS*4)**	
	θ	β	θ	β	θ	β	θ	β
High code	0.0200	0.40	0.0275	0.30	0.0500	0.30	0.0500	0.30
Medium code	0.0200	0.40	0.0025	0.30	0.0035	0.30	0.0035	0.30
Low code	0.0175	0.40	0.0225	0.40	0.0322	0.40		

Although the damage thresholds proposed by FEMA P-58 were derived based on experimental results, the specimens used are representative of those designed according to

US Codes and take into account the seismic intensities of the US area. Thus, the proposed thresholds of damage state can be viewed as similar to the CBA damage limit state.

1.4. Damage Limit State Based on FE Modeling

In the preceding sections, a variety of approaches have been briefly described to define the damage limit state. The experimental based approach has an advantage in terms of direct correlation between the response quantities and the observed damage. Hence, the defined limit state can be straightforwardly verified from the experiment. However, the experiment may encounter some difficulties to observe various detailed damage phenomena and can only capture the most obvious damage such as cracking. In this case, direct correlation between the observed damage and limit state at various levels may not be easily determined. The response quantities and the observed damage need to undergo rigorous analysis before they can be used for determining damage limit state [21–23].

Meanwhile, analytical method, performed on the basis of member-types model, can only provide responses which are expressed in term of deformation quantities. Thus, damage is interpreted by developing a damage model that relates the degree of damage to the deformation quantities. On the basis of the predicted degree of damage by the model, the damage limit state may be defined. Of course, the acceptability of the defined damage limit state is influenced by the accuracy of the damage model. No physical damage phenomena are available from the analytical method that otherwise can be useful to directly indicate the fitness of the proposed damage model. Generally, databases of damage that are relevant to the proposed model have to be collected from large experimental results to verify the model [29,30]. Unfortunately, there is no single damage model that can be broadly applied for all types of structure. A modification of the existing damage model may have to be proposed to properly estimate damage in special structures [40]. In some instance, damage database may not be available to calibrate the proposed damage model. In such situations, simulated damage from FE can be of help.

FE modeling offers an opportunity to fill the deficiency of both experiment and analytical approach as indicated above. FE modeling can simulate the detailed damage phenomena that the experiment and analytical method are not capable to observe. The FE modeling can generate the physical damages (cracking, yield strain, buckling, etc.) as well as the response quantities that account for the behavior of the structure. The ranges of output from the FE modeling can be exploited to directly correlate between the extent of damage and the structural behavior. Thus, the relationship between damage characteristics, EDP, and damage state as previously illustrated in Figure 1 can be created by FE modeling. The availability of this type of figure is helpful for identifying the damage limit state especially in the case of damage assessment of special structures. Even for a typical structure such as RC frame, the figure can be used to evaluate the validity of current damage limit state proposed by other methods. Of course, the capability of FE modeling to generate such results is determined by the appropriateness in the modeling which includes materials constitutive laws, numerical technique, and numerical/visualization of the FE results. All of these depend on the FE software. ATENA is FE software which is capable of simulating damage in RC accurately [41]. ATENA also has been applied to simulate seismic response of structures, which indicates the capability of the software to capture the behavior and damage in the investigated structures [42,43].

1.5. Fragility Curve

The damage limit state that has been properly defined will be useful for assessing the earthquake damage scenario of the structure. For this purpose, a fragility curve that describe the probability of reaching or exceeding different states of damage under earthquake excitation is constructed [9,12,20,28,44]. The output of fragility curve is an estimate of the cumulative probability of being in, or exceeding, each damage state for the given level of ground shaking. In addition, discrete damage state probabilities can be

created from the difference between the cumulative damage probabilities of the consecutive damage states for a given level of ground shaking [45,46].

Fragility curve is created by a median value of the potential earthquake hazard demand parameter that corresponds to the threshold of the damage state and by the variability associated with that damage state. The demand parameter for constructing the fragility curve can be a spectral displacement, drift ratio, or other engineering demand parameters. For a particular demand parameter, D_p, that defines the threshold of a particular damage state (ds), it is assumed to be distributed by [45]:

$$D_p = \overline{D_{p,ds}} \in_{ds} \tag{4}$$

where $\overline{D_{p,ds}}$ is the median value of demand parameter of damage state, ds; and ϵ_{ds} are a lognormal random variable with unit median value and logarithmic standard deviation, β_{ds}. In a more general formulation of fragility curves, the lognormal standard deviation, β has been expressed in terms of the randomness and uncertainty components of variability, β_R and β_U. Since it is not considered practical to separate uncertainty from randomness, the combined random variable term, β, is used to develop a composite "best estimate" fragility curve. A value of β_{ds} may be estimated using Equation (5) [34]:

$$\left.\begin{array}{l} \beta_{ds1} = 0.25 + 0.07ln(\mu_u) \\ \beta_{ds2} = 0.20 + 0.18ln(\mu_u) \\ \beta_{ds2} = 0.10 + 0.40ln(\mu_u) \\ \beta_{ds2} = 0.15 + 0.50ln(\mu_u) \end{array}\right\} \tag{5}$$

where μ_u is ductility, defined as ratio of deformation at ultimate to the yield state. For the CBA damage limit state, the β can be referred to the respected documents [39,45]. The conditional probability, P, of being in, or exceeding, a particular damage state, ds, given the demand parameter D_p, is defined by the function [45]:

$$P\left[ds\middle|D_p\right] = \Phi\left[\frac{1}{\beta_{ds}} \ln\left(\frac{D_p}{\overline{D_{p,ds}}}\right)\right] \tag{6}$$

where Φ is the standard normal cumulative distribution function

1.6. Objectives and Scope of the Study

The objective of this study is to evaluate damage limit state in RC frame based on FE modeling. 2D ATENA Engineering software is used to simulate the progressive damage in RC frame under increasing lateral load up to failure. The simulated damages will be characterized in term of concrete cracking and reinforcing bars strains. Based on the examination of these damage characteristics, the points corresponding to damage stages are plotted in the capacity curve of the investigated building. The curve provides a link between the damage and response quantities. The curve is then exploited to evaluate the fitness of damage limit states estimated by models that relates damage limit state with response quantities. Based on the evaluation, this study also proposes a modification of damage state threshold values. The capacity curve with its corresponding progressive damage from FE simulation will also be used to inspect whether the expected damage to the investigated building is within the range estimated by the CBA damage limit state.

The proposed damage threshold value will be used to quantify damage of the investigated building under design earthquake. So, this study includes assessing damage in RC frame under Design Basis Earthquake (DBE) and Maximum Considered Earthquake (MCE) scenario by mean of fragility curve.

2. Methods

2.1. Model Building Type

This study used a reinforced concrete frame from Kakaletsis [47] as a model building type to be investigated. Figure 2 illustrates the model building. The beam and column cross sections were 100 × 200 mm and 150 × 150 mm, respectively. The dimensions represent 1/3 scale of the prototype frame section, i.e., 300 × 600 mm for beams and 450 × 450 mm for

columns. Columns had tighter shear reinforcement along their length. Shear reinforcement in the beam was also closer in the critical area. In the beam-to-column joint, five horizontal stirrups were provided to prevent brittle shear failure. The diameter of 5.60 mm and 3 mm for longitudinal reinforcement and stirrup, respectively, correspond to the 1/3 scale of the 18- and 10-mm diameter bars of the prototype frame. In the specimens, low-strength plain reinforcement was used, although the rule of construction practice is to use high-strength deformation reinforcement. The material properties of the model structure are given in Table 3. The reinforced concrete frame represents a typical ductile concrete construction conforming seismic code.

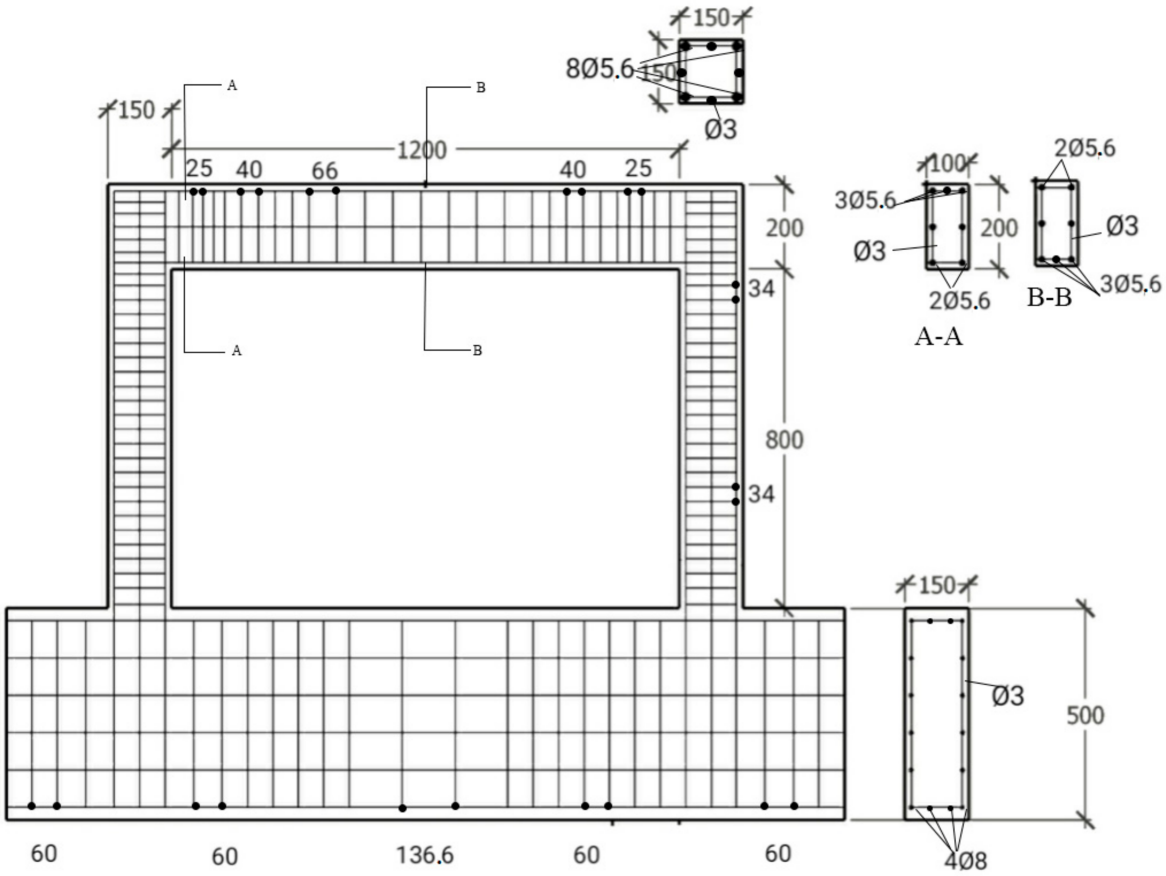


Figure 2. Model of building type.

Table 3. Properties of materials used.

Mechanical Properties	Value
Compressive strength of concrete f'_c	28.51 MPa
Yield/tensile strength of longitudinal reinforcement f_y/f_u	390/516 MPa/MPa
Yield/tensile strength of transverse reinforcement f_y/f_u	212/321 MPa/MPa

2.2. FE Modeling of the Investigated RC Frame

The Kakaletesis's model was analyzed using a finite element software, i.e., 2D ATENA Engineering. The responses of the model by the FE simulation were then validated using the experimental results of Kakaletsis.

In the software, the behavior of concrete is modeled as fracture-plastic model which combines constitutive models for tensile (fracturing) and compressive (plastic) behavior. The fracture model is based on the classical orthotropic smeared crack formulation and crack band model. It employs Rankine failure criterion, exponential softening, and it can

be used as rotated or fixed crack model. The hardening/softening plasticity model is based on Menétrey–Willam failure surface. This concrete constitutive model is defined as 3D Non-Linear Cementitious 2 in the ATENA.

Reinforcement can be modeled in two distinct forms: discrete and smeared. Discrete reinforcement is in form of reinforcing bars and is modeled by truss elements. For the current study, the discrete model is used. Meanwhile, the constitutive behavior of reinforcement bar follows the multi-linear law. This law allows to model all four stages of steel behavior: elastic state, yield plateau, hardening and fracture. The bond between reinforcing bar and the surrounding concrete is determined by the bond-slip relationship. For the current study, the bond-slip relationship according to the CEB-FIB model code 1990 is chosen.

In the numerical simulation by ATENA, the load is transferred into model structure via steel plate. In this way, the concentration of loads that might affect the fracture of concrete was eliminated. The behavior of the steel follows elastic isotropic law. Spring element is used to model spring-like boundary conditions for the foundation element of the structure in the horizontal direction.

In the ATENA program, solid element geometries are modeled as macro-elements. For the current model building, there are 7 (seven) macro-elements that have to be defined, where 6 (six) of which represents concrete elements i.e., 1 (one) beam element, 2 (two) column elements, 2 (two) joints elements, and 1 (one) foundation element. The other macro-element is used to represent a steel plate for load transfer. Connections between macro-elements are defined by surface contact with perfect connection type. Meanwhile, the line elements are used to geometrically model the reinforcement bars embedded in the macro-elements of concrete.

The meshing process of the model structure into small finite elements is automatically carried out in the ATENA software (Figure 3). The basic elements that can be selected for meshing are brick, tetra and brick-tetra combinations. The tetra element has a higher order of analysis compared to brick. The main consideration in choosing the finite element model is laid on the computational complexity. Basically, a simpler model is preferable as long as the results are sufficiently representative. Considering this, the brick element is chosen in this study.

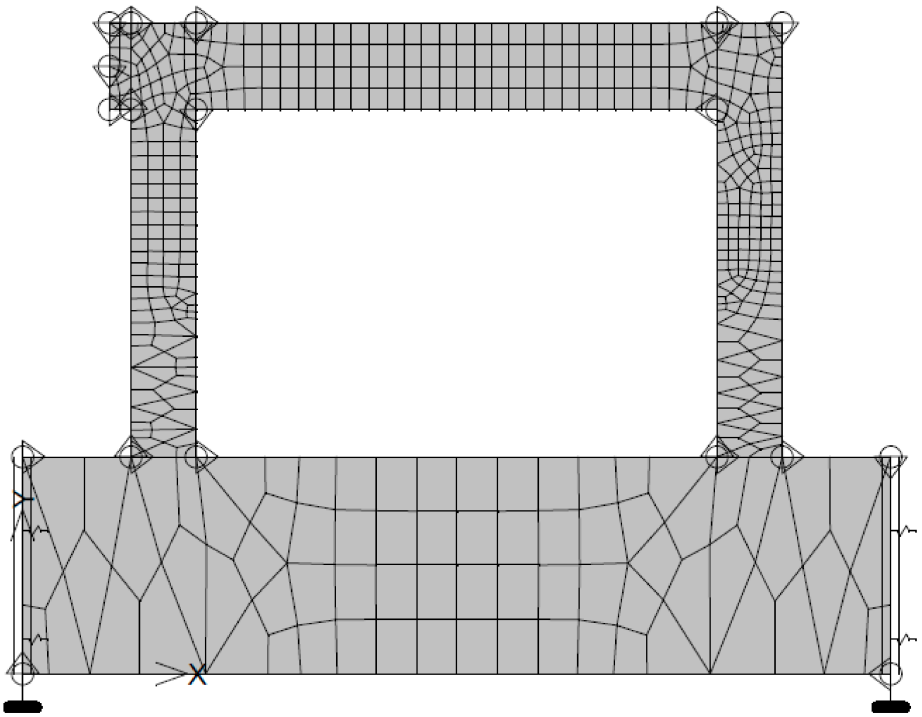


Figure 3. FE model of the investigated frame structure.

In Kakaletsis's experiment, a lateral load was applied to the model structure by means of a double action hydraulic actuator. Full reversal of loading on the model structure was applied by displacement control where the displacement was gradually increased. Seven displacement amplitude sets of two loading cycles per set were used to load the RC frame horizontally. The cycles started from a ductility level of 0.8 corresponding to an amplitude of approximately ±2 mm and were followed gradually by ductility levels of 2, 4, 6, 8, 10, and 12 corresponding to amplitudes of 6, 12, 18, 24, 30, and 36 mm. The hysteretic response envelope was drawn and presented as lateral load-displacement. For the current study, lateral load is applied incrementally by displacement control instead of quasi-static lateral cyclic loading. Therefore, the obtained response of FE simulation will be validated by the response envelope of Kakaletsis's result.

3. Results and Discussion

3.1. Validity of FE Modeling

Before we utilize the results of the FE simulation for assessing the damage state of the example reinforced concrete frame, first, we need to validate them with the experimental results. Structural response of the model building obtained from FE modeling is presented in Figure 4, together with the experimental result of Kakaletsis. Generally, the FE model gives a very close load-displacement behavior to that of the Kakaletsis. The similarity of the curves suggests that many engineering parameters that can be deduced from the two curves are comparable. The global structural responses of the model structure indicate ductile failure modes; even though the maximum displacement of the FE model is slightly lower than the experimental result. The cracks intensities and their corresponding positions that occur at failure is also comparable to that of Kakaletsis's experiment (see Figure 5). The similarity can indicate the same failure mechanism between the FE model and Kakaletsis's experiment.

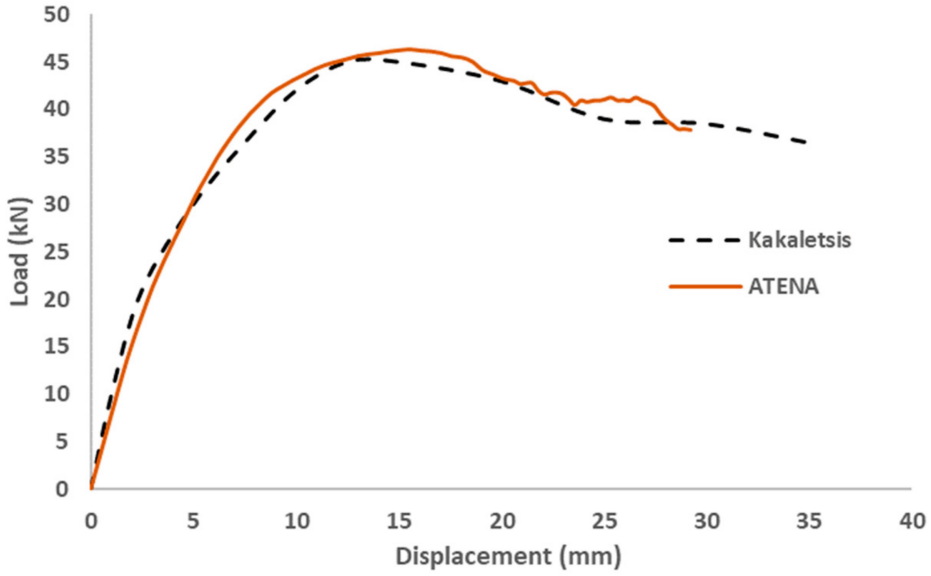
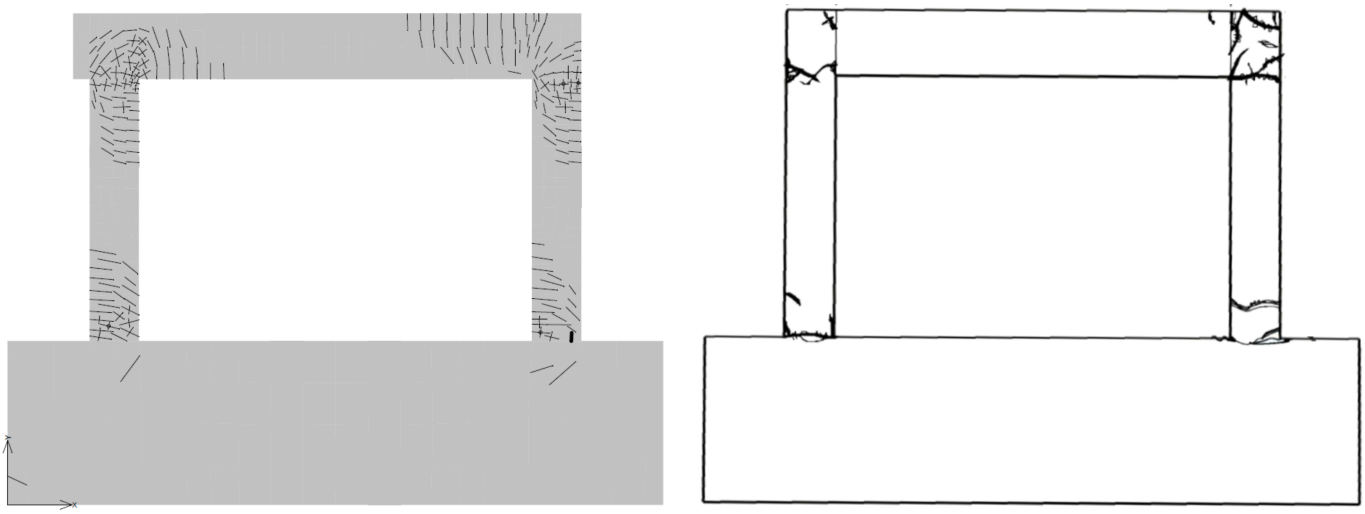


Figure 4. Load-displacement of the building model.

3.2. Progressive Damage

The lateral load-displacement curve illustrates the response of the model structure when the structure sustains a seismic load. The shape of the curve represents the behavior of the structure under loading. At early loading stage, a linear load-displacement can be expected to indicate a linear-elastic behavior of the structure before any damages are induced (Figure 6). Inspection of Figure 4, one can deduce that both FE simulation and Kakaletsis's experiment suggest the limit of linear-elastic behavior occurs at a load of about 20 kN. This limit can be assumed to resemble the first appearance of the cracks (Figure 7a).

After this loading stage, a linear relationship of the load-displacement still be expected but the curve shows a lesser stiffness due to the propagation and increasing intensity of cracks as load increases. At a load of about 35 kN, the first yielding of the reinforcing bars is observed at the bottom of the columns (Figure 7b). Loading of the model structure beyond this load up to the peak load causing more formation and propagation of cracks and also a greater number of the yielded reinforcing bars including those at the upper columns (Figure 7c). When the concrete starts to crush due to high compression stress, the compression zones lost their capability to sustain stress. In turn, a higher stress is transferred to the compression reinforcing bars. These bars start to yield as observed in the bottom columns (Figure 7d). At this state, the curve displays a drop of load as displacement increases. The structure still capable to behave in ductile manner before the compression bars are buckling (Figure 7e). The points of the progressive damages as mentioned above have been plotted in the load-displacement curve (see Figure 6); and Figure 7 provides the supporting data of the damages corresponding to the stated points of damages.



(**a**) (**b**)

Figure 5. Comparison of cracks intensities of the FE results (**a**) and Kakaletsis's experiment (**b**).

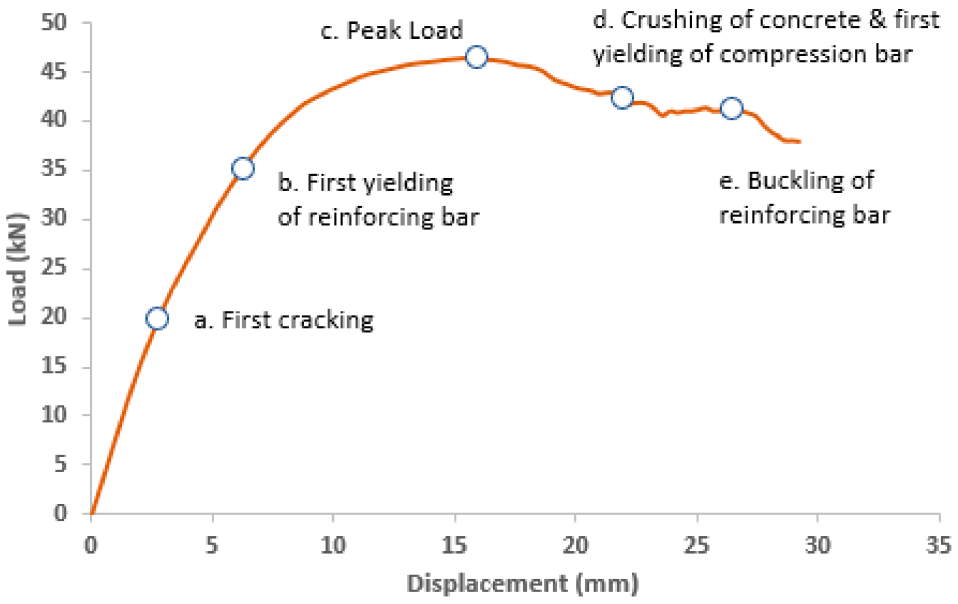
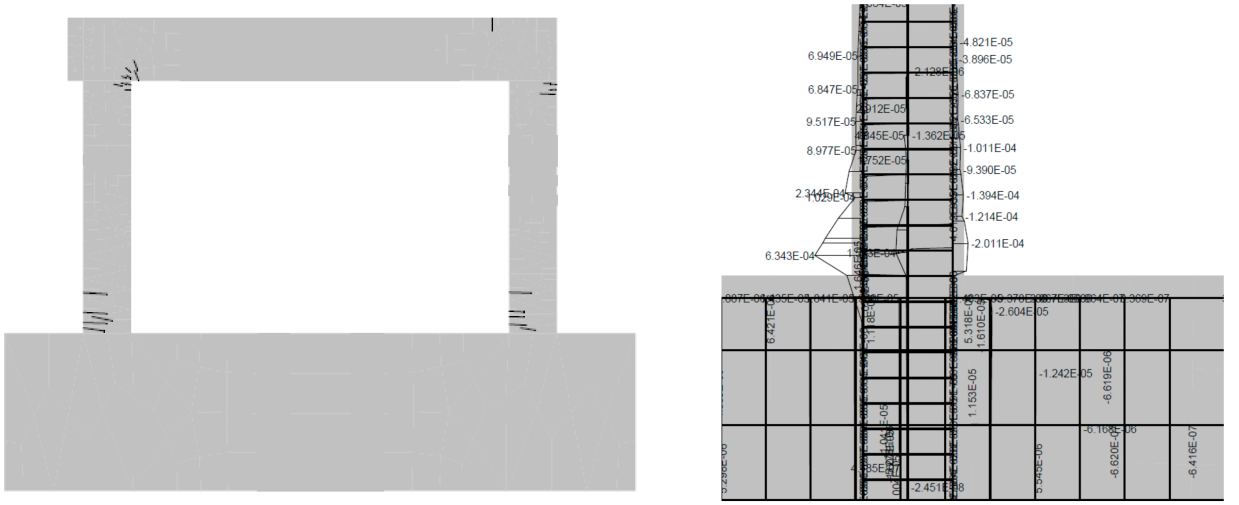
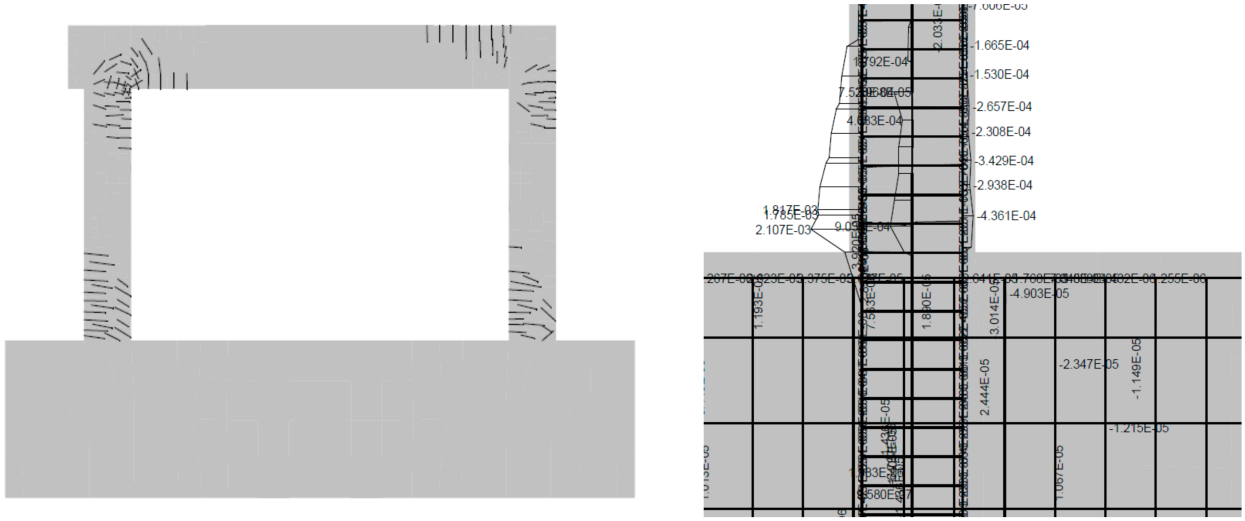


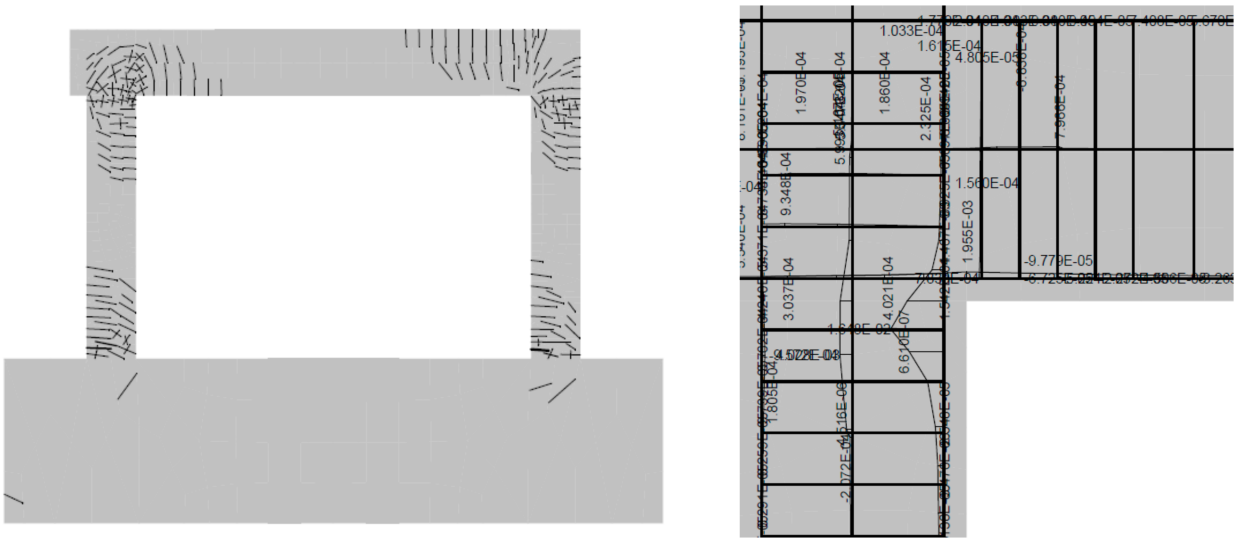
Figure 6. Points of progressive damage.



(**a**)



(**b**)



(**c**)

Figure 7. *Cont*.

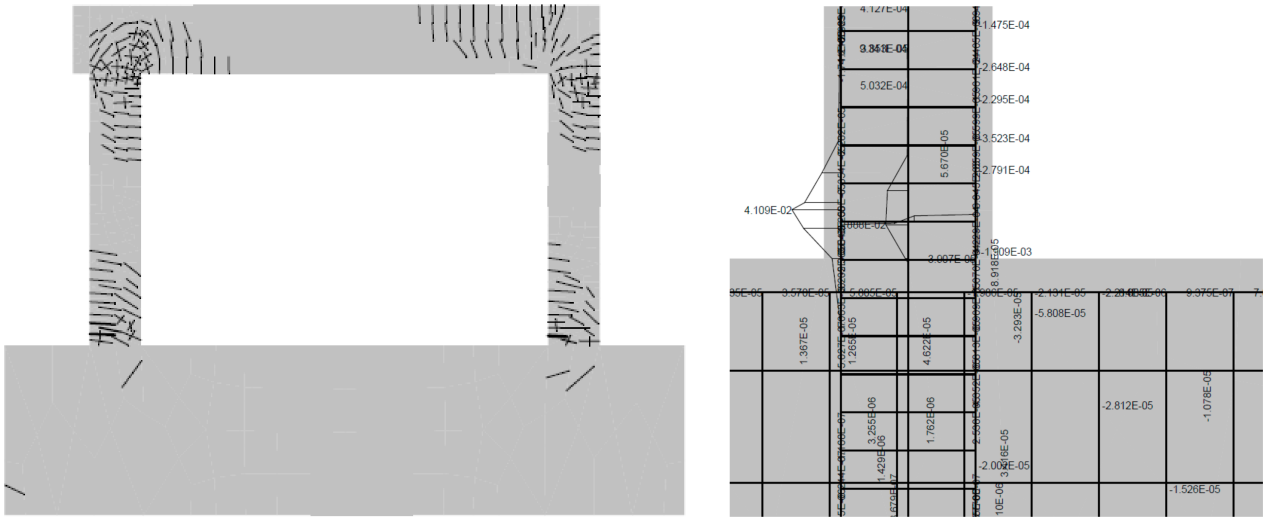


Figure 7. The progressive damages in term of concrete cracking and crushing as well as yielding and buckling of the reinforcing bars. (**a**) At a load of 20 kN, fine cracks appear at locations with high intensity of tensile stresses. The corresponding maximum tensile strain of the reinforcing bars (at the bottom column) at this load level is 6.343×10^{-4}, which is still below the yield strain (1.95×10^{-3}). (**b**) At a load of 35 kN, more formation of fine cracks appeared and first yielding of the reinforcing bars at the bottom of columns is observed. The maximum reinforcement strain at this location reaches 2.107×10^{-3} which is above the yield strain. (**c**) At a peak load, more cracks and a greater number of yielded reinforcing bars (including at the upper column) are observed. (**d**) At a post-peak, significant cracks in the compression zones may lead to crushing of concrete especially at the bottom columns and in turn, higher stresses are transferred to the compression reinforcing bars. Consequently, compression reinforcing bars start to yield as indicated by the maximum compression strain in these bars reaching -1.909×10^{-3}. (**e**) Some of the yielded compression reinforcements at the bottom columns may start to buckle. The strain of the compression reinforcements reaches -4.763×10^{-3} at a load of 40 kN after peak-load.

3.3. Control Points

Two control points can be identified directly by inspection of point in the load-displacement curve corresponding to the first yielding of reinforcing bar and the sign of buckling of reinforcing bar, respectively. As stated in the previous section, from Figure 7b,e, respectively, the occurrence of the first yielding and buckling of reinforcing bars can be

identified. These points have already been plotted in the load-displacement curve as shown in Figure 6. This direct identification of control points is compared with the two other approaches i.e., the concept of reduced stiffness equivalent elasto-plastic yield (shown in Figure 8a) and equivalent elasto-plastic energy absorption (shown in Figure 8b). For the purpose of analysis, the trend of the curve is converted into polynomial equation order 3 by regression analysis. The estimated equation is:

$$L = 0.0067D^3 - 0.4181D^2 + 7.8785D \quad (7)$$

where L = Load (kN) and D = displacement (mm). The correlation coefficient, R^2 of Equation (7) is 0.9948. Table 4 shows the values of the control points determined by the above methods. It confirms all methods give close estimation of control points; the difference is not more than 3%.

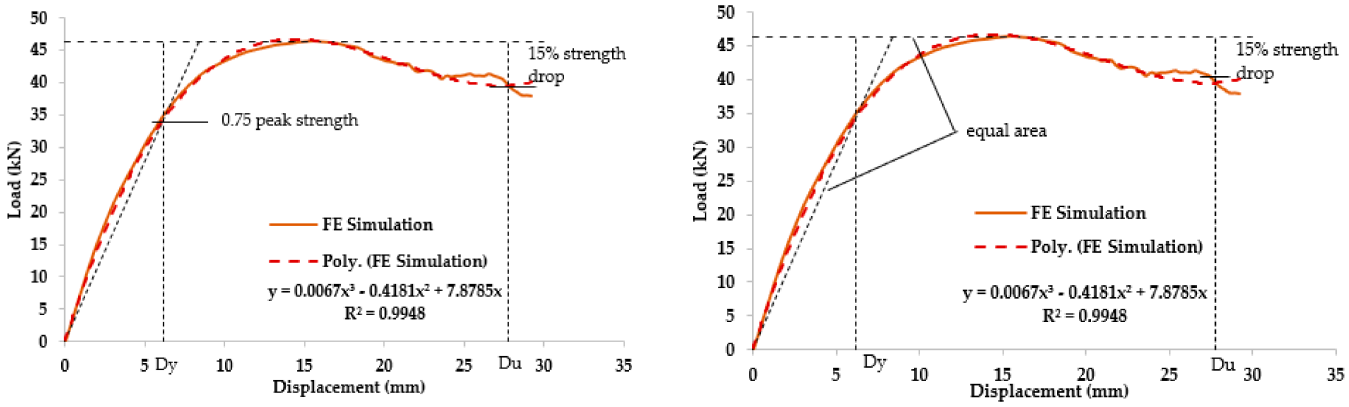


Figure 8. Analytical approach to determine control points. (**a**) Reduced stiffness equivalent elasto-plastic yield. (**b**) Equivalent elasto-plastic energy absorption.

Table 4. Control points of the load-deformation curve.

Method	Δy (kN)	Δy (mm)	Δu (kN)	Δu (mm)	$\Delta y/\Delta y$ *	$\Delta y/\Delta u$ *
FE simulation	35.00	6.40	41.00	26.55	1.00	1.00
Reduced stiffness	34.75	6.31	39.38	27.33	0.99	1.03
Equivalent energy absorption	34.37	6.21	39.38	27.33	0.97	1.03

* based on FE simulation.

3.4. Damage Limit State

The definition of damage limit state according to Equation (1) will be evaluated in this section. Control points as given in Table 4 are used for estimating the damage limit state. Since the estimated control points by three methods are barely different, so control points determined from FE simulation will be used for estimating and evaluating the damage limit state. The results are plotted in the load-displacement curve as shown in Figure 9. It should be noted that the threshold calculated by Equation (1) is the upper limit of the respective damage state.

The minimum limit state to account for damage is *DS*0. Below this level, structure is considered undamaged. Referring to Figure 9, it is shown that threshold value of *DS*0 is already passing the point of first cracking. It seems necessary to lower the threshold of *DS*0, so any cracks that appear below this level are not neglected. *DS*1 (slight damage) falls within the cracking point and yielding point. FE simulation can confirm that at this range, damage is characterized by hairline flexural cracks which appear in both beam and column near the joints as well as at the bottom column (Figure 7b). *DS*2 (medium damage) is defined after first yielding of the tensile reinforcing bars. Examination of the *DS*2 threshold value suggests that the limit corresponds to about 86% peak strength. At this

point, the flexural crack intensity can be observed over a larger area. Strains in reinforcing bars are increased including the one that has yielded. The increase in strain causes some of them (other than the previous yielded reinforcement) about to attain a yielding limit. This description of damage can be checked from the FE simulation. *DS*3 (extensive damage) is at a point approaching the peak strength. At this point, more reinforcing bars are already yielding. The RC frame is just about to lose its capacity due to concrete crushing where the concrete compression strain attains 1.85×10^{-3}. *DS*4 (very heavy damage) lays at a point after concrete crushing and compression reinforcement yielding. RC frame has passed its plastic capacity. Thus, the damage is irrecoverable.

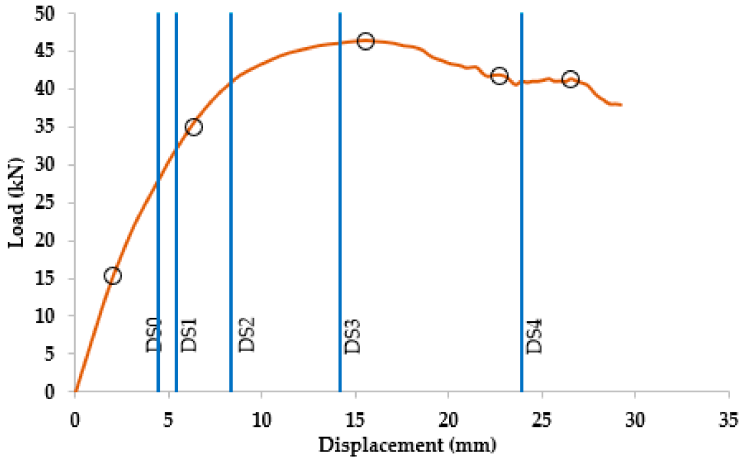


Figure 9. Damage limit state according to Equation (1).

The second damage limit state that will be evaluated is that of defined by Equation (2). Since the control points are expressed in term of spectral displacement, the curve of Figure 6 needs to be converted into capacity spectrum following the procedure of ATC 40 [48]. The control points given in Table 4 (FE simulation) will also be converted first into spectral displacement and then used to estimate the threshold value of *DS*1 to *DS*4 according to Equation (2). The results are plotted in the capacity spectrum curve as shown in Figure 10. Note that the threshold is the lower limit.

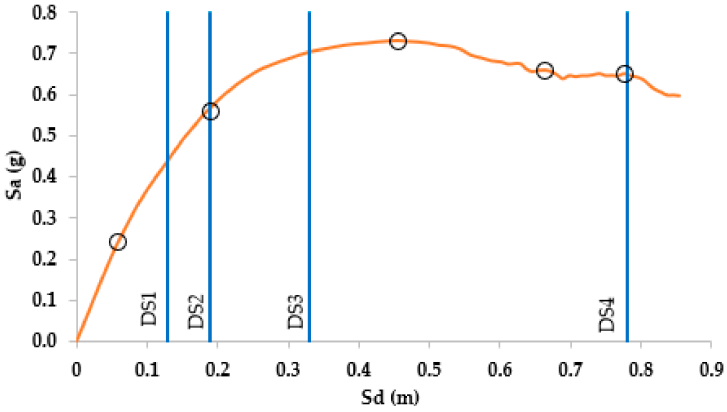


Figure 10. Damage limit state according to Equation (2).

The lower limit of slight damage (*DS*1) lays between first cracking and yielding point. Basically, this lower limit is similar to the upper limit of *DS*0 in Figure 9. This limit is the minimum threshold value for the structure to be considered damaged. It means cracks that can be identified when the structure undergoes seismic load above the cracking load are neglected. Lowering the threshold value of *DS*1 may be reasonable to minimize the expected cracks that is considered to be harmless. Medium damage is determined by *DS*2 and *DS*3, which is the lower and upper threshold value, respectively. *DS*2 coincides with

the first yielding of reinforcing bar while *DS*3 is about 73.5% of the spectral displacement at peak. Generally, RC frame is designed to demonstrate a ductile behavior where the frame can still take a higher load (about 25%) after first yielding. Assigning yield point as the lower limit and 73.5% of spectral displacement at peak as the upper limit of medium damage can be considered appropriate. Meanwhile, extensive damage is defined to be between *DS*3 and *DS*4. At *DS*4, some reinforcing bars already exhibit buckling. It seems to be rational to lower the threshold value of *DS*4 in order to prevent the failure of RC frame due to buckling. Buckling should only be expected at complete damage.

Based on the above evaluation, the following damage limit state is proposed. First, the lower limit of slight damage (*DS1*) should be reduced to control cracks that appear above cracking load. The displacement at cracking point of the investigated structure is 2.7 mm. Setting *DS*1 at 3.2 mm (equals to 20% above the cracking point) is acceptable to limit the cracks that are considered harmless. This point is about 50% of the displacement at yield point. The limit can also be expressed in term of drift ratio of 0.36% or spectral displacement of 0.09 m. *DS*2 and *DS*3 may be set similar to Equation (2) for the reason stated in the preceding paragraph. *DS*4 should be set in such a way to prevent structural collapse due to buckling. A point just after the appearance of concrete crushing may be selected as the curve shows the structure still possess some degree of ductility. Considering this, *DS*4 is assigned at spectral displacement of 0.70 m which equals to 90% of ultimate spectral displacement (D_u). So, Equation (2) is modified to Equation (8):

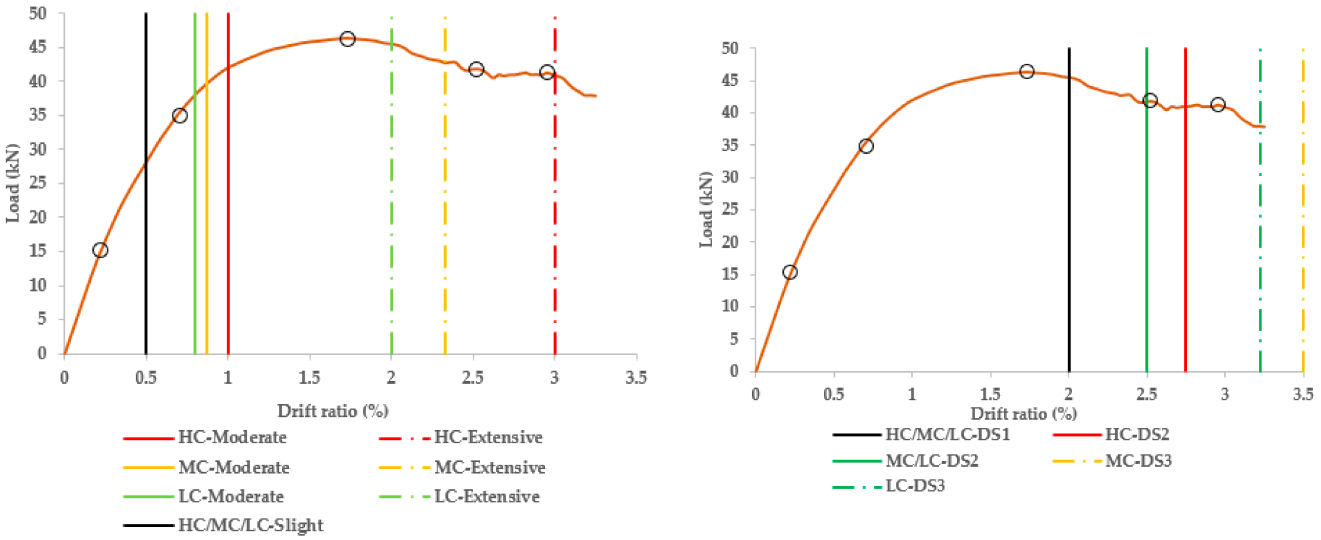
$$\left.\begin{array}{l} DS1 = 0.5D_y \\ DS2 = D_y \\ DS3 = D_y + 0.25(D_u - D_y) \\ DS4 = 0.9D_u \end{array}\right\} \quad (8)$$

3.5. CBA Damage Limit State

One of the uses of the CBA damage limit state is to indicate if a structure has been designed to meet the expected damage under design earthquake scenario. If the damage is more severe than the CBA's set, then it indicates that the structure is weak. This can be carried out by inspecting the position of the CBA damage threshold within the capacity curve of the investigated structure. The CBA damage limit states to be used for the current case study are those of Hazus-MH 2.1 and FEMA P-58. It should be noted that the defined threshold values proposed by Hazus-MH 2.1 and FEMA P-58 as shown in Tables 1 and 2, respectively, are expressed in term of interstory drift ratio. Hence, the lateral load-displacement curve as shown in Figure 6 is converted into lateral load-drift ratio. Figure 11 shows the lateral load-drift ratio of the model structure. The threshold values of the damage states criteria from Hazus-MH 2.1 and FEMA P-38 are also shown in the figure.

The slight damage limit state of Hazus either for high-code (HC), medium-code (MC), or low-code (LC) falls between the first and second points of progressive damage of the curve. At this drift ratio (0.5%), the physical damage of the structure can be expected to be in the forms of fine cracks without any yielding of the reinforcing bars. So, the slight damage of the Hazus criteria is met. The same is for the moderate damage where the threshold value of this state of damage for HC, MC, or LC falls between the second and third points of progressive damage of the curve. At this state of damage, some of the reinforcing bars are already yielding, but the structure still be able to redistribute the stresses in such a way so it can sustain higher load. For the extensive damage state, it seems the threshold value of HC is too high. At drift ratio of 3%, the structure already experiences buckling. So, this threshold value cannot be met by the structure. However, the structure can tolerate the extensive damage criteria set for both MC and LC design level. At drift ratio of 2.33%, crushing of concrete can be expected to occur. In addition, many reinforcing bars have reach the yielding limit either due to tensile or compression stress. However, at this extensive state of damage, the structure still shows some extents of ductile behavior. The last damage state defined by Hazus, i.e., complete is not plotted in the figure since the

drift ratio of 5–8% is far beyond the expected ductility of the structure. The structure is collapse at drift-ratio of 3.25%.



(**a**) (**b**)

Figure 11. The threshold value of damage states defined by Hazus-MH 2.1 (**a**) and FEMA P-58 (**b**) in the load-drift ratio curve.

Meanwhile, the damage states *DS*1 and *DS*2 of FEMA P-58 stay at the post peak response of the load-drift ratio curve, even for LC design level. It does not seem realistic to expect slight and medium damage can be met by the structure at the defined damage states of FEMA P-58. Additionally, most of the *DS*3 and *DS*4 threshold values are beyond the expected failure of the model structure. In conclusion, the structure cannot meet the expected damage set by the FEMA P-58 criteria as the damage is more severe.

3.6. Fragility Curve

This section is dedicated to evaluating the estimated damage that may occur in the model structure due to the design earthquake based on the fragility curve. The building site chosen to represent the seismic intensity is the Surakarta region, Indonesia. The design response spectrum of this region can be accessed via this reference link [49].

The first step in developing the fragility curve is to convert the capacity curve of Figure 6 into capacity spectrum following the procedure of ATC 40 [48]. The result is presented in Figure 9 as spectral acceleration (Sa) vs. spectral displacement (Sd). The next step is to apply the proposed damage states criteria as set in Equation (8). Table 5 shows the estimated damage limit state by Equation (8).

Table 5. Damage state for developing fragility curve.

Engineering Parameter	Damage State			
	Slight	**Medium**	**Extensive**	**Complete**
Spectral displacement (m)	0.09	0.19	0.33	0.70

The threshold values of damage states set in Table 5 are used to plot the fragility curves as lognormal cumulative probability functions by means of Equation (6). The procedure for constructing fragility curve can be summarized as follows [34]:

a. Define the capacity spectrum of the model structure (Figure 12);
b. Identify and determine the control points using one of the methods described in sub-Section 3.3;

c. Define the damage limit state using Equation (8). For the current case of study, the obtained value is given in Table 5;
d. Define the β_{ds} parameter using Equation (5). The estimated parameter may be refined to better respresent the logical damage order. For example, when the estimated β_{ds} for complete damage is too high (0.86), it may cause the probability of this damage state is higher than the extensive damage state, especially at the low range of spectral displacement. For this reason, the β_{ds} parameter for the complete damage state is set similar to the extensive damage state i.e., 0.67;
e. Apply Equation (6) for a range of spectral displacement covering the probable seismic intensities of the region.

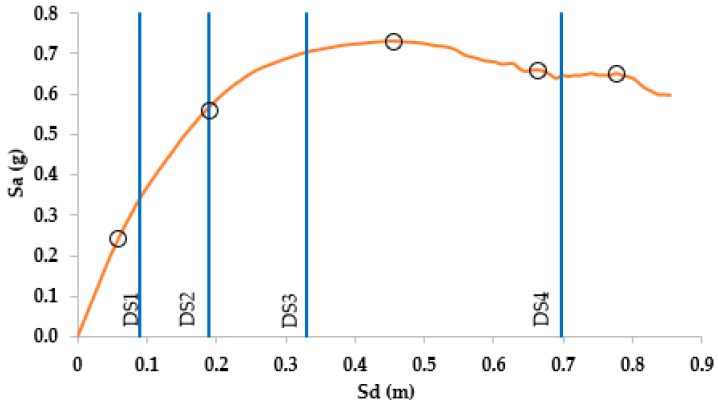


Figure 12. A plot of damage state threshold in the capacity spectrum.

The resulting fragility curves are presented in Figure 13. For the purpose of assessing seismic fragility, design earthquake levels of Design Basis Earthquake (DBE) and Maximum Considered Earthquake (MCE) are specified. The DBE and MCE are determined following procedure set out in the Indonesian Standard (SNI 1726:2019) [50]. The important parameters to be considered for determining the design earthquake levels of DBE and MCE are peak ground acceleration, soil type, structure risk category, etc. These parameters are related to the building site. Originally, the design earthquake are presented as a spectral acceleration response given in this reference link [49]. This spectrum is converted into spectral displacement demand. The specified spectral displacement demand for DBE and MCE levels are plotted as well in Figure 13.

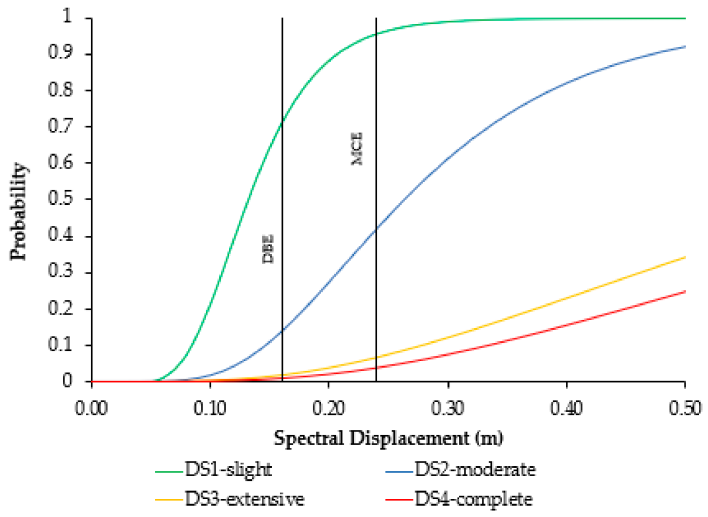


Figure 13. Fragility curve at various damage state levels.

Figure 13 provides information on the extent of damages that will be expected to occur in the model building when an earthquake at a level of DBE or MCE strikes the structure. The expected damages can be presented using discrete damage probabilities which are calculated as the difference of the cumulative probabilities of reaching, or exceeding, successive damage states [45]. Based on the fragility curves of Figure 13, the discrete damage probabilities have been obtained and given in Figure 14. At DBE, the probability of slight damage is equal to 57% and moderate damage is 12%. This indicates that under DBE, the probable damage that can be expected in the model structure in the form of harmless flexural cracks is 57%. There are only 12% possibilities for the structure to exhibit damage in the form of yielding reinforcement. Meanwhile, at MCE the corresponding probability is 53% and 35% for slight and moderate damage, respectively. The probability of damage at moderate level is increased by 23% from the design earthquake level of DBE to MCE. No significant damage at extensive and complete level is expected under earthquake at DBE level. While the total probability of extensive and complete damage under earthquake at MCE level is 4.65%.

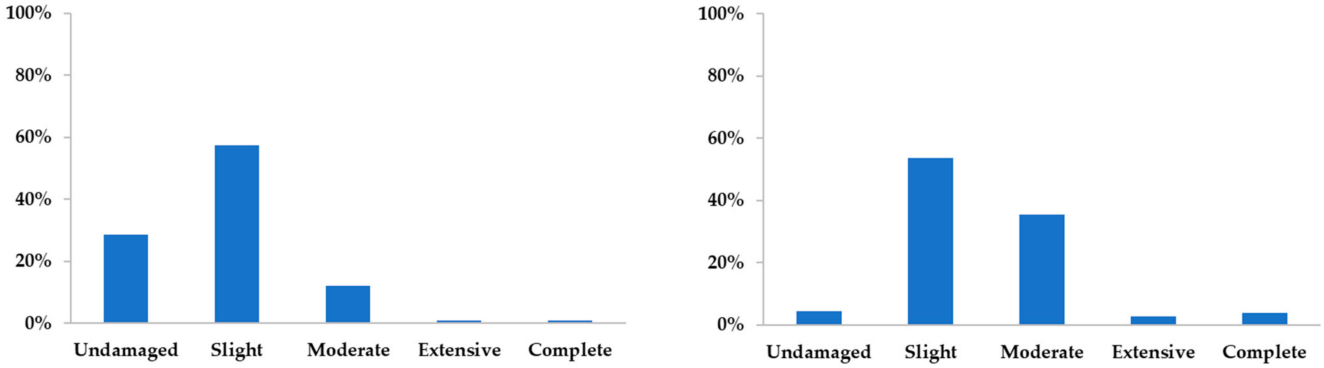


Figure 14. Discrete damage probabilities of the model building due to design earthquake of DBE (**a**) and MCE (**b**).

4. Conclusions

Various damage limit states have been proposed in the literatures to define the expected of damage in the building due to seismic action at a variety of intensities. This study evaluates those damage limit states based on the FE modeling results. FE modeling provides the lateral load-displacement behavior of the model structure together with the corresponding progressive damages. The following findings are highlighted:

a. Two control points corresponding to the first yielding and buckling of reinforcement point can be identified from the FE simulation results. The estimated control points are very close to the prediction by the method of reduced stiffness equivalent elasto-plastic yield and equivalent elasto-plastic energy absorption;
b. Damage states defined on the basis of model which relates the limit state with the control points such as Equations (1) and (2) generally are reasonable as confirmed by the simulated damage of FE modeling. However, a refinement of limit state for *DS*1 and *DS*4 is proposed in this study. The refinement of *DS*1 aims to limit the expected cracks that may occur at this damage level, while the refinement of *DS*4 is intended to reduce the upper limit of extensive damage to the point before structure collapses. The capability of FE modeling to simulate damage and identify the limit state based on that damage is useful for proper definition of the limit state. This method can be extended for other structures, especially for non-typical structure where a model for estimating damage limit state is absent;
c. The simulated damage from FE modeling has also been used to identify the level of damage that may occur in the model structure compared to the CBA damage limit

state such as that of Hazus-MH 2.1 and FEMA P-58. More severe damage is indicated in the model structure than what is required by Hazus-MH 2.1 and FEMA P-58. The assessment of damage by the above principle can serve as first indication whether a structure has been sufficiently designed to meet the expected code performance or not;

d. The fragility curve has been presented to quantify the probability of damage that can be expected in the model structure based on a set of damage limit state proposed in this study. In the case of this research, the most probable damage in the structure falls in the category of slight if earthquake at a level of DBE or MCE strikes the structure. However, at MCE level the probability of moderate damage attains 53% or an increase of 23% compared to the DBE level.

Author Contributions: S.A.K. contributed to the original conception, performed numerical simulation, analyzed data, and wrote initial draft of the manuscript; I.R.H. analyzed data, and reviewed the draft; E.P. analyzed data, and reviewed the draft; M.M. carried out drawing, and reviewed the draft. All authors have read and agreed to the published version of the manuscript.

Funding: This research was funded by MINISTRY of RESEARCH and TECHNOLOGY, INDONESIA via Research Assignment of PTNBH under program Fundamental Research Grant, contract number 221.1/UN27.22/HK.07.00/2021.

Institutional Review Board Statement: Not applicable.

Informed Consent Statement: Not applicable.

Data Availability Statement: The data presented in this study are available on request from the corresponding author.

Conflicts of Interest: The authors declare no conflict of interest.

References

1. Applied Technology Council. *FEMA P-154 Rapid Visual Screening of Buildings for Potential Seismic Hazards: A Handbook*; Applied Technology Council: Wahsington, DC, USA, 2015.
2. Jain, S.K.; Mitra, K.; Kumar, M.; Shah, M. A proposed rapid visual screening procedure for seismic evaluation of RC-frame buildings in India. *Earthq. Spectra* **2010**, *26*, 709–729. [CrossRef]
3. Tama, Y.S. Structural damages observed in state buildings after Simav/Turkey earthquake occurred on 19 May 2011. *Nat. Hazards Earth Syst. Sci.* **2012**, *12*, 2709–2718. [CrossRef]
4. Dolce, M.; Goretti, A. Building damage assessment after the 2009 Abruzzi earthquake. *Bull. Earthq. Eng.* **2015**, *13*, 2241–2264. [CrossRef]
5. Ozmen, H.B. Relation between the rapid evaluation method scores and the damage states of buildings. *Nat. Hazards Earth Syst. Sci.* **2013**, *13*, 763–770. [CrossRef]
6. Ruggieri, S.; Cardellicchio, A.; Leggieri, V.; Uva, G. Machine-learning based vulnerability analysis of existing buildings. *Autom. Constr.* **2021**, *132*, 103936. [CrossRef]
7. Zheng, R.; Xiong, C.; Deng, X.; Li, Q. Assessment of Earthquake Destructive Power to Structures Based on Machine Learning Methods. *Appl. Sci.* **2020**, *10*, 6210. [CrossRef]
8. Baltzopoulos, G.; Baraschino, R.; Iervolino, I.; Vamvatsikos, D. SPO2FRAG: Software for seismic fragility assessment based on static pushover. *Bull. Earthq. Eng.* **2017**, *15*, 4399–4425. [CrossRef]
9. Melani, A.; Khare, R.K.; Dhakal, R.P.; Mander, J.B. Seismic risk assessment of low rise RC frame structure. *Structures* **2016**, *5*, 13–22. [CrossRef]
10. Biglari, M.; Formisano, A.; Davino, A. Seismic vulnerability assessment and fragility analysis of Iranian historical mosques in Kermanshah city. *J. Build. Eng.* **2021**, *45*, 103673. [CrossRef]
11. Del, C.; Marco, G.; Ludovico, D.; Polese, M.; Manfredi, G.; Prota, A.; Ricci, P.; Verderame, G.M. *Seismic Fragility for Italian RC Buildings Based on Damage Data of the Last 50 Years*; Springer: Berlin/Heidelberg, Germany, 2019; ISBN 0123456789.
12. Hapsari, I.R.; Sangadji, S.; Kristiawan, S.A. Seismic performance of four-storey masonry infilled reinforced concrete frame building. In *MATEC Web of Conferences*; EDP Sciences: Les Ulis, France, 2018; Volume 195, p. 02017.
13. Erberik, M.A. Seismic Fragility. In *Encyclopedia of Earthquake Engineering*; Beer, M., Kougioumtzoglou, I.A., Patelli, E., Au, S.-K., Eds.; Springer: Heidelberg, Germany, 2015; ISBN 9783642353437.
14. Kappos, A.J. Seismic damage indices for RC buildings: Evaluation of concepts and procedures. *Prog. Struct. Eng. Mater.* **1997**, *1*, 78–87. [CrossRef]

15. Elenas, A.; Meskouris, K. Correlation study between seismic acceleration parameters and damage indices of structures. *Eng. Struct.* **2001**, *23*, 698–704. [CrossRef]
16. Kostinakis, K.; Athanatopoulou, A.; Morfidis, K. Correlation between ground motion intensity measures and seismic damage of 3D R/C buildings. *Eng. Struct.* **2015**, *82*, 151–167. [CrossRef]
17. Ohkubo, M. *Current Japanese System on Seismic Capacity and Retrofit in Techniques for Existing Reinforced Concrete Buildings and Post-Earthquake Damage Inspection and Restoration Techniques*; Department of Applied Mechanics & Engineering Sciences, University of California: San Diego, CA, USA, 1991.
18. Nakano, Y.; Maeda, M.; Kuramoto, H.; Murakami, M. Guideline for post-earthquake damage evaluation and rehabilitation of RC buildings in Japan. In Proceedings of the 13th World Conference on Earthquake Engineering, Vancouver, BC, Canada, 1–6 August 2004; Volume 15.
19. Maeda, M.; Al-Washali, H.; Matsukawa, K. An overview of post earthquake damage and residual capacity evaluation for reinforced concrete buildings in Japan. In Proceedings of the Pacific Conference on Earthquake Engineering, Auckland, New Zealand, 4–6 April 2019; Volume 1, pp. 930–943. [CrossRef]
20. Hamid, N.H.A.; Mohamad, N.M. Seismic assessment of a full-scale double-storey residential house using fragility curve. *Procedia Eng.* **2013**, *54*, 207–221. [CrossRef]
21. Carrillo, J.; Alcocer, S.M. Backbone Model for Performance-Based Seismic Design of RC Walls for Low-Rise Housing. *Earthq. Spectra* **2012**, *28*, 943–964. [CrossRef]
22. Carrillo, J.; Alcocer, S.M. Acceptance limits for performance-based seismic design of RC walls for low-rise housing. *Earthq. Eng. Struct. Dyn.* **2012**, *41*, 2273–2288. [CrossRef]
23. Carrillo, J.; Dominguez, D.; Prado, N. Seismic Damage Index Based on Fractal Dimension of Cracking on Thin Reinforced Concrete Walls. *ACI Struct. J.* **2017**, *114*, 1649–1658. [CrossRef]
24. Ning, N.; John, Z.; Zhang, P.; Yu, D.; Wang, J. Influence of masonry infills on seismic response of RC frames under low frequency cyclic load. *Eng. Struct.* **2019**, *183*, 70–82. [CrossRef]
25. Ahmad, N.; Shahzad, A.; Ali, Q.; Rizwan, M. Seismic fragility functions for code compliant and non-compliant RC SMRF structures in Pakistan. *Bull. Earthq. Eng.* **2018**, *16*, 4675–4703. [CrossRef]
26. Shiradhonkar, S.R.; Sinha, R. Validation of seismic damage states for reinforced concrete buildings. In Proceedings of the NCEE 2014-10th US National Conference on Earthquake Engineering: Frontiers of Earthquake Engineering, Anchorage, AK, USA, 21–25 July 2014. [CrossRef]
27. Sohn, J.; Choi, I.; Kim, J. Development of limit states for seismic fragility assessment of piloti-type structures verified with observed damage data. *Eng. Struct.* **2022**, *251*, 113562. [CrossRef]
28. Dimova, S.L.; Negro, P. Seismic assessment of an industrial frame structure designed according to Eurocodes. Part 2: Capacity and vulnerability. *Eng. Struct.* **2005**, *27*, 724–735. [CrossRef]
29. Panagiotakos, T.B.; Fardis, M.N. Deformations of Reinforced Concrete Members at Yielding and Ultimate. *ACI Struct. J.* **2002**, *98*, 135–148.
30. Park, Y.; Ang, A.H. Mechanistic seismic damage model for reinforced concrete. *J. Struct. Eng.* **1985**, *111*, 722–739. [CrossRef]
31. Fu, G.; Liu, B. The Research on Modified Park-Ang Damage Model Based On Effective Energy Dissipation. *Adv. Mater. Res.* **2013**, *742*, 46–50. [CrossRef]
32. Ang, A.H. Seismic damage assessment and basis for damage-limiting design. *Probabilistic Eng. Mech.* **1988**, *3*, 146–150. [CrossRef]
33. Soleymani, A.; Safi, M. Correlations between Damage Indices and Seismic Parameters for Near-Field Earthquake Records. *Civ. Eng. Dimens.* **2015**, *16*, 75–86. [CrossRef]
34. Milutinovic, Z.V.; Trendafiloski, G.S. RISK-EU an Advanced Approach to Earthquake Risk Scenarios with Applications to Different EUROPEAN Towns. *WP4 Vulnerability Curr. Build*. **2003**. Available online: http://www.civil.ist.utl.pt/~{}mlopes/conteudos/DamageStates/Risk%20UE%20WP04_Vulnerability.pdf (accessed on 1 December 2021).
35. Vargas, Y.F.; Pujades, L.G.; Barbat, A.H.; Hurtado, J.E. Incremental Dynamic Analysis and Pushover Analysis of Buildings. A Probabilistic Comparison. *Comput. Methods Appl. Sci.* **2013**, *26*, 293–308. [CrossRef]
36. FEMA. *Earthquake Loss Estimation Methodology, Hazus-MH 2.1. Advanced Engineering Building Module (AEBM), Technical and User's Manual*; FEMA: Washington, DC, USA, 2015.
37. FEMA-NIBS. *HAZUS Earthquake Model Technical Manual, Hazus 4.2 SP3*; FEMA-NIBS: Ottawa, ON, Canada, 2020.
38. Naderpour, H.; Mirrashid, M. A novel definition of damage states for structural elements in framed reinforced concrete buildings. *J. Build. Eng.* **2020**, *32*, 101479. [CrossRef]
39. Applied Technology Council. *FEMA P-58 Seismic Performance Assessment of Buildings*; Applied Technology Council: Redwood City, CA, USA, 2018.
40. Guo, J.; Wang, J.J.; Li, Y.; Zhao, W.G.; Du, Y.L. *Three Dimensional Extension for Park and Ang Damage Model*; Elsevier: Amsterdam, The Netherlands, 2016; Volume 7, pp. 184–194. [CrossRef]
41. Cervenka, V.; Cervenka, J.; Pukl, R.; Sajdlova, T. Prediction of Shear Failure of Large Beams Based on Fracture Mechanics. In Proceedings of the 9th International Conference on Fracture Mechanis of Concrete and Concrete Structures FraMCoS-9, Prague, Czech Republic, 29 May 2016.
42. Ahmed, A.; Shahzada, K. Seismic vulnerability assessment of confined masonry structures by macro-modeling approach. *Structures* **2020**, *27*, 639–649. [CrossRef]

43. Do, A.; Livao, R.; Uluda, C.E.; Faculty, C.E.; Do, A.; Livao, R.; Do, A.; Uluda, C.E.; Faculty, C.E.; Do, A.; et al. Comparison and assessment of material models for simulation of infilled RC frames under lateral loads. *Građevinar* **2019**, *71*, 45–56.
44. Saruddin, S.N.A.; Nazri, F.M. Fragility curves for low- and mid-rise buildings in Malaysia. *Procedia Eng.* **2015**, *125*, 873–878. [CrossRef]
45. FEMA. *Multi-Hazard Loss Estimation Methodology, Earthquake Model, Hazus–MH 2.1: Technical Manual*; FEMA: Washington, DC, USA, 2012.
46. Kircher, C.A.; Nassar, A.A.; Kustu, O.; Holmes, W.T. Development of building damage functions for earthquake loss estimation. *Earthq. Spectra* **1997**, *13*, 663–682. [CrossRef]
47. Kakaletsis, D.J.; Karayannis, C.G. Experimental investigation of infilled reinforced concrete frames with openings. *ACI Struct. J.* **2009**, *106*, 132–141. [CrossRef]
48. Applied Technology Council. *ATC-40 Seismic Evaluation and Retrofit of Concrete Buildings*; Applied Technology Council: Redwood City, CA, USA, 1996; Volume 1.
49. Direktorat Bina Teknik PUPR Desain Spektra Indonesia. Available online: http://rsa.ciptakarya.pu.go.id/2021/index.php?pga=0.3489&ss=0.7974&s1=0.3863&tl=20&kelas=4&range=6#grafik (accessed on 1 December 2021).
50. Badan Standarisasi Nasional. *SNI 1726:2019 Tata Cara Perencanaan Ketahanan Gempa Untuk Struktur Bangunan Gedung Dan Nongedung*; Badan Standarisasi Nasional: Jakarta, Indonesia, 2019.